**Article:**
Bird, A., Yang, L. orcid.org/0000-0003-0935-3921, Wu, G. et al. (1 more author) (2023) Failure mechanisms of diamond like carbon coatings characterised by in situ SEM scratch testing. Wear, 530-531. 205034. ISSN 0043-1648

https://doi.org/10.1016/j.wear.2023.205034

# Failure mechanisms of diamond like carbon coatings characterised by in situ SEM scratch testing

A. Bird [a,*], L. Yang [b], G. Wu [b], B.J. Inkson [a,**]

[a] Department of Materials Science and Engineering, The University of Sheffield, Sheffield, S1 3JD, UK
[b] Institute of Functional Surfaces, School of Mechanical Engineering, University of Leeds, Leeds, LS2 9JT, UK

ARTICLE INFO

*Keywords:*
Diamond like carbon
DLC
In situ scanning electron microscopy
Scratch testing
Failure mechanisms

ABSTRACT

In situ SEM scratch testing of DLC and Si-doped DLC deposited on Si < 100> wafers has been conducted using sharp 1 and 5 μm radii diamond asperities, enabling the stages of deformation and wear of DLC coatings to be evaluated in real time. With increasing load, initial plastic deformation and tensile cracking in the scratch track progresses to the propagation of radial and lateral cracks, and full coating spallation. In situ SEM imaging reveals nucleation of radial cracks in the DLC coating around the front and side of the moving asperity, followed by lateral crack propagation both ahead of, and behind, the asperity contact zone. Post-mortem FIB cross sectioning reveals microcracking and lateral cracks in the silicon substrate below DLC coatings prior to coating spallation. The DLC failure mechanisms are influenced by asperity geometry, with notable DLC coating lift up/delamination events occurring during the smaller 1 μm radius asperity scratch tests. The sharper 1 μm radius asperity required ~20% of the applied load, and higher contact pressure, to initiate spallation during scratching compared the larger 5 μm asperity, indicating that smaller radii asperities are significantly more likely to cause DLC coating spallation, although the spallations they generate were observed to be, on average, smaller.

## 1. Introduction

Diamond like carbon (DLC) covers a wide range of amorphous carbon-based coatings [1,2], which have gained extensive interest in recent times [3–6]. Their excellent tribological properties and wear resistance make them ideal for use in areas of high reciprocating wear [4,6,7]. Favourable dry lubricant properties also allow them to be utilised in areas where traditional wet lubrication is not an option [8]. The performance of a DLC coating depends on a range of microstructural factors including the substrate used, use of interlayers [9] and the $sp^3/sp^2$ ratio of the coating [10]. Additionally the use of dopants, such as Si, has been shown to modify the bonding, friction and wear behaviour of DLC coatings [5,8,11]. With such a wide array of potential variants, understanding the wear and behaviour of DLC coatings is not a straightforward task.

DLC coatings have been traditionally evaluated using nano- and micro-scratch testing, with post-mortem wear analysis being used to interpret wear mechanisms from residual damage [12–14]. The development of in situ SEM mechanical testing has opened up new opportunities for dynamical observation of friction and wear mechanisms of coatings at the nanoscale [15], enabling changes in mechanical properties to be directly linked with specific microstructural changes in the coatings under test. In this work, we use both in situ SEM and conventional scratch testing with small asperity diamond tips to evaluate the factors that influence the wear and failure of thin coating DLC coatings on Si < 100> wafers. The tribology and wear of two undoped DLCs and a Si-doped DLC are compared, to characterise the influence of DLC chemistry and coating thickness on the failure mechanisms under the presented scratch conditions.

## 2. Experimental

### 2.1. DLC coating deposition

Three different DLC coatings were fabricated for tribological evaluation using plasma enhanced chemical vapor deposition (PECVD). Single side polished silicon <100> wafers, 72.2 mm in diameter and 380 μm thick, were used as the substrate material. For coating a Hauzer Flexicoat® 850 multipurpose platform industrial coater was used, coating the polished side of the Si wafers with no interlayers.

* Corresponding author.
** Corresponding author.
*E-mail addresses:* ADBird1@sheffield.ac.uk (A. Bird), beverley.inkson@sheffield.ac.uk (B.J. Inkson).

Immediately before coating the samples were ultrasonically cleaned for 15 min with acetone and ethanol respectively, samples were mounted on sample holders inside the chamber. The vacuum chamber was then pumped down to reach a base pressure of 5.0 × 10 -6 mbar. The Si substrates were then cleaned for 30 min using a plasma source (Ar gas). The dopant free DLCs were deposited by PECVD in separate runs using acetylene gas (purity, 99.5%) at around 200 °C. The Si doped DLC was deposited by PECVD using acetylene gas and Hexamethyldisiloxane (HMDSO) at around 200 °C. Deposition time for both was about 45 min.

### 2.2. Coating evaluation

Cross sections of the DLC coated wafers were made using a Ga + focus ion beam (FIB) equipped scanning electron microscope (FIB-SEM, Helios NanoLab G3, FEI). Cross sections were also made by splitting the Si-wafers with dicing pliers and imaging them on a 90° SEM stub using SEM (Nova 450 SEM, FEI). Surface topography was measured by 3D optical profilometry (Contour GT, Bruker).

The surface mechanical properties of the coatings were evaluated by nanoindentation (Micromaterials Nano test vantage), using a 1 mN load, load rate of 0.1 mN $s^{-1}$, and hold time of 10 s using a diamond Berkovich tip. A Renishaw InVia Raman Microscope was used for Raman analysis of the DLC coatings pre and post-test. A 50x objective lens with an excitation wavelength of 514 nm at 2 mW laser power was used, with two acquisitions and a 15 s exposure time for each scan. XPS analysis was conducted on a Kratos Supra with a monochromated Al source (1486.6eV) with two data collection areas of 700 μm and 300 μm. Survey scans were collected between 1200 and 0eV binding energy, 160eV pass energy, and 1eV intervals. High resolution scans were collected at 20 eV pass energy with 0.1eV interval sweeps for each analysis point over an appropriate energy range with a 300 s sweep.

### 2.3. Ex situ scratch testing

A Micro Materials NanoTest Vantage was used for ex situ scratch testing of the DLC coatings, fitted with a friction probe to give 3-axis lateral force measurements during scratch testing. A 5 μm radius diamond conical tip was used for all tests. Scratch speed was set to 0.5 $\mu ms^{-1}$, and ramp and un-ramp rates were 1 $mNs^{-1}$ with a max load of 250 mN held for 30 s. For each scratch test a pre-test and post-test topographical scan was taken at the same scratch speed with a load of 0.1 mN.

### 2.4. In situ scratch testing

In situ SEM scratch testing took place using an Alemnis nanoindenter inside a FEI Nova 450 SEM. Here both 1 μm and 5 μm radius diamond spheroconical tips were used in scratch testing experiments, with a load/unload rate of 1 $mNs^{-1}$ and a scratch speed of 0.5–1 μm $s^{-1}$. Max load was determined by the critical load of the given sample under test. All scratch tests were imaged in situ using concurrent secondary electron (SE) imaging.

## 3. Results

### 3.1. DLC coating evaluation

The three different amorphous DLC coatings fabricated, DLC-1, DLC-2 and Si-DLC, were characterized by FIB-SEM, Raman and XPS. The measured coating thickness values were DLC-1 510 nm, DLC-2 260 nm, and Si-DLC 620 nm. DLC-2 was noticeably thinner than its counterparts, allowing for coating thickness comparisons throughout the testing.

The surface roughness of the DLC-1, DLC-2 and Si-DLC coatings was characterised by 3D optical profilometry (Bruker Contour GT) (Fig A1). Each coating displayed similar arithmetical mean height ($S_a$) values with DLC-1 being measured at 9±1 nm, DLC-2 at 6±1 nm and Si-DLC 8±1 nm. Each coating was observed to have occasional cavitations and defects within the surface, likely caused by the PECVD coating process itself as the substrate was lithography grade Si.

Analysis of the Raman spectroscopy carbon D (disorder) and G (graphite) peaks from the DLC-1, DLC-2, and Si-DLC coatings are summarized in Table 1. The ratio of the D and G peak intensities $I_D/I_G$ enables an evaluation of $sp^3$ to $sp^2$ hybridised carbon within each coating. $I_D/I_G$ for DLC-1 and DLC-2 were measured at 0.48 and 0.72 respectively, consistent with a reduced level of $sp^2$ carbon present in DLC-1. Si-DLC had an $I_D/I_G$ of 0.37, consistent with an even lower level of $sp^2$ hybridised carbon within the coating. Additionally, DLC-1 and DLC-2 had G peak positions of 1549 $cm^{-1}$ and 1559 $cm^{-1}$ respectively, whereas the introduction of a Si dopant saw the G peak for Si-DLC drop to 1514 $cm^{-1}$. This reduction in $I_D/I_G$ ratio and G peak wavenumber with the Si doping of DLCs is consistent with other values reported in the literature [8].

Chemical composition (excluding hydrogen) of the coating surface was evaluated using XPS (Table 2). DLC-1 and DLC-2 displayed a greater carbon content at 88.8 and 91 (at% of the detected elements) respectively, with Si-DLC showing a lower overall carbon content at 74.8 (at %). DLC-2 incorporated higher residual Ar from the PECVD process. All samples displayed oxygen content at the surface, with DLC-1 9.5 (at%), DLC-2 7.8 (at%), and Si-DLC higher at 14.6 at%. The increased oxygen level at the coating surface of the Si-DLC has been reported previously due to the affinity of the Si within the coating to oxidise [16,17].

### 3.2. DLC mechanical properties

The mechanical properties of the DLC-1, DLC-2 and Si-DLC coatings were measured by nanoindentation (Fig. 1), and compared to an uncoated <100> Si-wafer reference sample. Average hardness was calculated across 25 indents per sample. From the 1 mN load indentation tests, DLC-1 can be seen to have the overall greatest hardness at 18.8 ± 2.5 GPa, with DLC-2 having an average hardness of 17.5 ± 2.8 GPa (Fig. 1(a,c)). Si-DLC showed significantly lower hardness at 14.2 ± 2.1 GPa on average, with the uncoated reference Si wafer's hardness being measured at 10.9 ± 2.6 GPa. On average DLC-1 and DLC-2 had similar elastic properties, with an average reduced modulus $E_r$ of 159 ± 12 GPa and 149 ± 12 GPa respectively (Fig. 1(b and c)). Si-DLC showed a decrease in average $E_r$, at around 122 ± 12 GPa. The $H/E_r$ ratios for all three DLC coatings were comparable at 0.12 (Fig. 1(d)).

### 3.3. Ex situ scratch testing of DLC-1, DLC-2 and Si-DLC

Conventional nanoindenter scratch testing of the DLC-1, DLC-2 and Si-DLC coatings was conducted up to a maximum load of 250 mN, using a 5 μm radius spheroconical diamond tip. Fig. 2 shows representative tipdisplacement under load curves for a scratch test on each coating, together with a post-test topographical scan of the residual scratch tracks. 3D optical profilometry was used post mortem to image the residual scratch track topography of repeated tests on each coating (Fig. 3).

Plastic deformation of the DLC coatings due to the diamond scratching is clearly visible in the optical profilometry, consisting of a linear scratch track, pile-up to the sides of the track as the scratch depth increases, and a distinct central zone of deep pits and some uplift in the

**Table 1**
Raman analysis of each DLC coating displaying the D and G peak positions ($cm^{-1}$), the full width half maximum (FWHM) of the G peak ($cm^{-1}$) and the peak intensity $I_D/I_G$ ratio taken from the surface of each sample.

| Coating | D peak position ($cm^{-1}$) | G peak position ($cm^{-1}$) | FWHM G | $I_D/I_G$ |
|---|---|---|---|---|
| DLC 1 | 1372 | 1549 | 176 | 0.48 |
| Si-DLC | 1357 | 1514 | 178 | 0.37 |
| DLC-2 | 1388 | 1559 | 158 | 0.79 |

**Table 2**
XPS surface elemental analysis of each sample DLC-1, DLC-2 and Si-DLC; values are given as at % of the detected elements.

| Sample | Na | Zn | O | N | C | Ar | Ca | Si | S |
|---|---|---|---|---|---|---|---|---|---|
| **DLC 1** | 0.3 | 0.2 | 9.5 | 0.2 | 88.8 | <0.1 | 0.3 | 0.4 | 0.2 |
| **Si-DLC** | 0.7 | <0.1 | 14.6 | 0.5 | 74.8 | <0.1 | <0.1 | 9.3 | <0.1 |
| **DLC 2** | 0.2 | <0.1 | 7.8 | 0.4 | 91 | 0.7 | <0.1 | <0.1 | <0.1 |

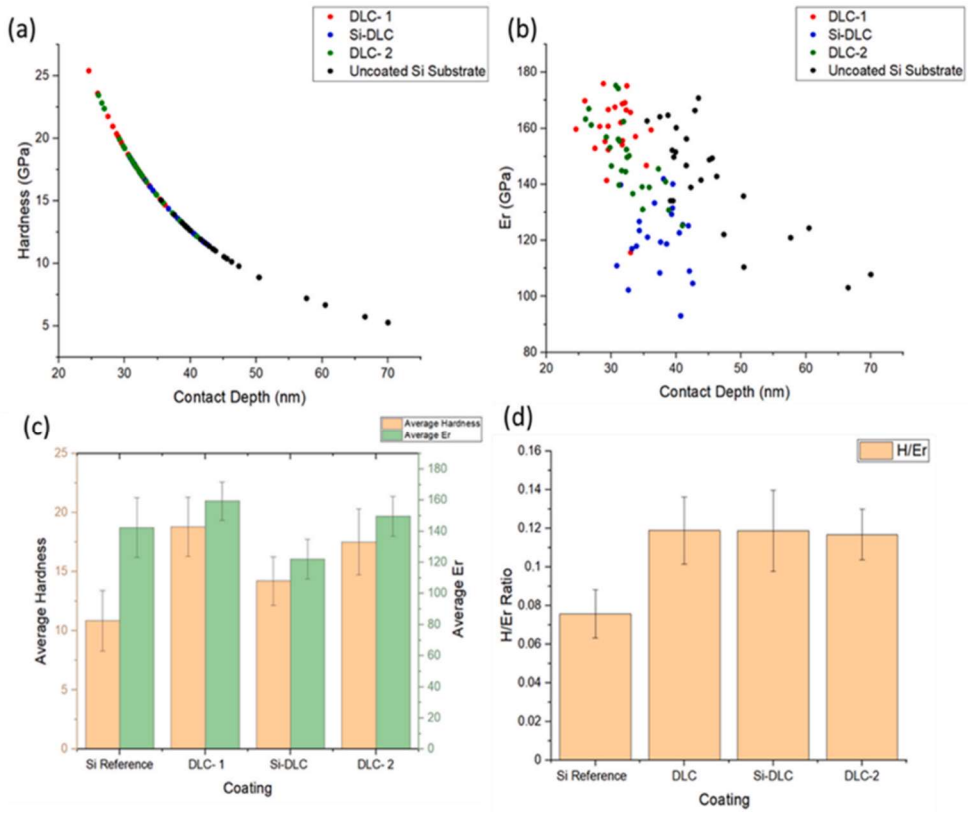


**Fig. 1.** 1 mN nanoindentation testing of DLC-1, Si-DLC, DLC-2, and an uncoated reference Si wafer. (a) Hardness (H) as a function of indentation contact depth. (b) Reduced modulus ($E_r$) as a function of contact depth. (c) Comparison of average hardness and reduced modulus between samples. (d) Average hardness over reduced modulus ($H/E_r$) ratios.

coating due to the onset of cracking, spallation and delamination at high load. A substantial amount of wear debris can be identified on the Si and DLC coating surfaces, concentrated around the central zone of maximum wear and towards the end of the wear track.

Each DLC coating, and the Si reference, displayed multiple craters from lateral spallation events (Fig. 3). There were distinct differences between the two undoped DLCs. DLC-1 displayed a large band of deep spallation in the central >2 μm length of the scratch where the load was above a critical load of approximately 184 mN sufficient to trigger this (Fig. 3(b)). The thinner DLC-2 however displayed only a few deep spallations, but with shallow damage along a longer length of scratch after a critical load of ~155 mN was surpassed (Fig. 3(d)).

Periodic penetration of the diamond indenter into the DLC-1 sample as a result of the large spallation events can be observed in the under-load scratch depth plots (Fig. 2), and in the post-test residual topography scans (Fig. 3(b)). In comparison, the thinner DLC-2 exhibited much smoother under-load scratch depth plots (Fig. 3(d)) due to infrequent spallation events. The Si-DLC coating (Fig. 3(c)) behaved in a similar manner to DLC-1 with regards to spallation. Once a critical load of approximately 226 mN had been surpassed large lateral spallations occurred along the edge of the Si-DLC scratch track until the ramp down phase of the test (Fig. 3(c)).

Post-mortem analysis of both width of spallation across the DLC scratch tracks, and the length of a given scratch exhibiting spallation, was conducted for the 5 μm radius ex situ scratch tests (Table 3). Spallation width was measured perpendicular to the scratch direction, being the distance between maximum extension of the spallations either side of the scratch. Note that post-mortem the spallation width includes the width of the central scratch track, as the moving tip cuts through the forward-facing spallation craters (see Section 3.3). Spallation width measurements were taken at 30%, 50% and 70% of the length of a scratch exhibiting spallation to sample a range of the load profile. The length of scratch exhibiting spallation was measured from 3D optical profiles of the wear scars, and Vision 64 software used to obtained

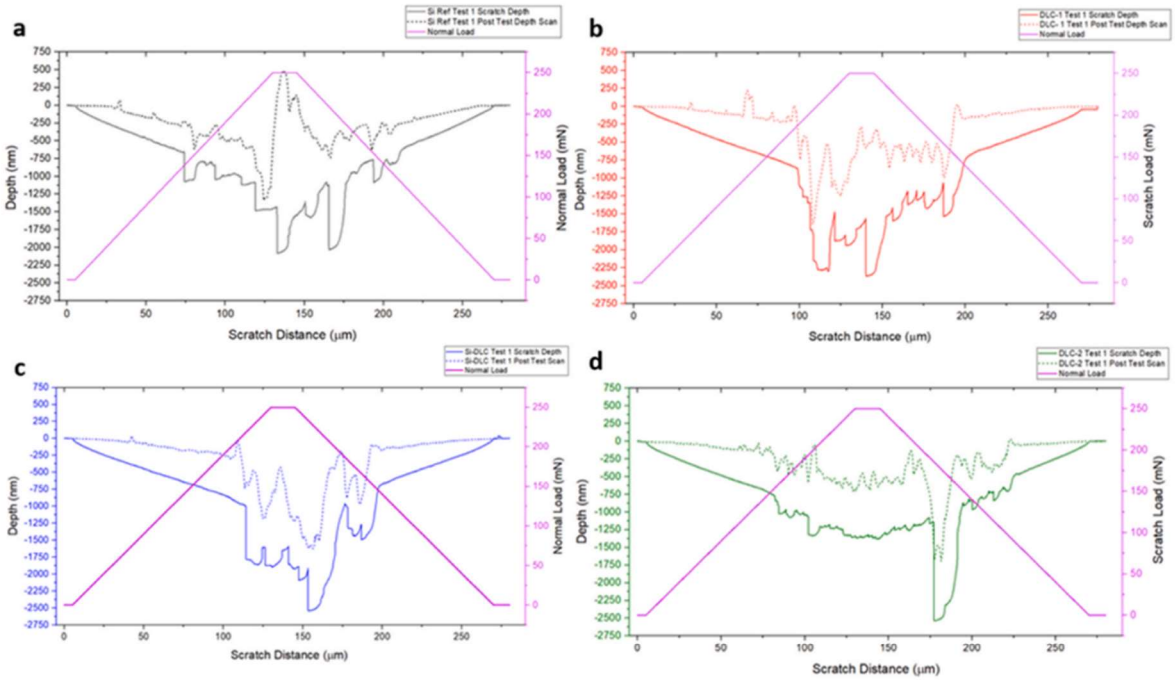


**Fig. 2.** Applied load, tip displacement (depth) and post-test topography plotted against scratch distance for scratch 1 of the ex situ scratch tests for each sample shown in Fig. 3. (a) Si reference sample. (b) DLC-1. (c) Si-DLC. (d) DLC-2. The applied normal load is plotted against scratch distance (pink line). (For interpretation of the references to colour in this figure legend, the reader is referred to the Web version of this article.)

precise measurements of the spallated wear scar. The analysis confirms that for the same scratch conditions the thinner DLC-2 coating exhibits a longer, narrower band of residual spallation damage compared to the thicker DLC-1 and Si-DLC coatings (Table 3). The DLC-1 and Si-DLC coatings have similar average width of spallation damage, but the Si-DLC spallation damage is shorter (Table 3).

The dynamical coefficient of friction (CoF) was determined during the diamond-DLC scratch tests (Fig B1). The Si reference sample showed a steady increase in CoF from 0.16 to 0.23 at the point just before spallation, with the CoF remaining at 0.15 in the ramp down phase of the test. The DLC-1, Si-DLC and DLC-2 scratch tests followed very similar patterns for CoF outside of the spallation zone, with a CoF between 0.12 and 0.14 in the pre-spallation phase, and a CoF of 0.1 in the ramp down phase. Inside the spallation zone all samples displayed erratic CoF values, ranging from 0.02 to 0.37, caused by the periodic spallation events causing fluctuations in local contact conditions and the indenter ploughing through the Si substrate. The DLC-2 coating did record slightly smoother CoF curves due to the coating's lesser tendency to spallate, with prolonged periods at a CoF of 0.2. However, in areas where spallation did occur DLC-2 CoF peaks up to 0.37 were recorded.

### *3.4. In situ SEM scratch testing of DLC-1, DLC-2 and Si-DLC with 5 μm radius diamond tip*

To evaluate the dynamical plastic deformation mechanisms taking place during DLC scratch testing, the surface mechanical properties of the DLC coatings were evaluated by nanoindenter scratch testing inside a scanning electron microscope.

Scratch testing of the DLC coatings was first conducted with 5 μm radius diamond spheroconical tips at a load rate of 1 $mNs^{-1}$, and a scratch speed of 0.5 $\mu ms^{-1}$, comparable with the ex situ scratch tests. Fig. 4(a–f) shows a representative time-resolved sequence of plastic deformation occurring during a 5 μm radius diamond conical scratch test on DLC-1. Initially, the DLC-1 plastically deforms under the tip and small cracks occur in the coating within the wear track. As the load and indenter depth increases, fractures start to occur in front of the tip, (Fig. 4(a), at a load of 188 mN, which extend out of the wear scar after the tip has passed over (Fig. 4(b)). As the load increases, cracks ahead and to the side of the tip contact zone propagate radially and laterally and a ~1 μm spallation occurs in front of the tip (Fig. 4(b), load 206 mN). Two seconds/1 μm sliding distance further on, a larger ~5 μm spallation occurs radially ahead of the indenter tip (Fig. 4(c), load 208 mN).

Once the load is sufficient to initiate DLC coating spallation, the softer Si substrate is unprotected in the spallation crater, and the diamond tip ploughs into the Si substrate (Fig. 4(d–f)). As the tip moves laterally forward, reaching fresh DLC coating, new cracks occur, and spallations continue to form in a "bow wave" like manner at the leading edge of the tip-DLC contact zone. The widening and growth of cracks and spallation behind the indenter as the compressive and tensile stresses are relaxed was observed (Fig. 4(f)).

Post-mortem SEM imaging enables closer examination of the wear scar in the scratch phase prior to spallation that was blocked from view during the test (Fig. 4(g and h)). In the run up to spallation of the DLC coating, tensile cracking with concave curvature occurs within the wear scar. As the load increases the residual cracking becomes both more frequent, and starts to extend radially outwards into the DLC coating surrounding the wear scar. In the few microns before onset of spallation of the DLC coating, the longer residual radial cracks extending outside the wear scar correlate with the observed initiation and propagation of cracks ahead and around the tip contact zone (e.g. Fig. 4(a)), and their growth as the tip passes (Fig. 4(b)). Once spallation started and the tip began to plough into the Si substrate exposed by the spallation craters, severe damage occurred until the scratch test was halted (Fig. 4(h)).

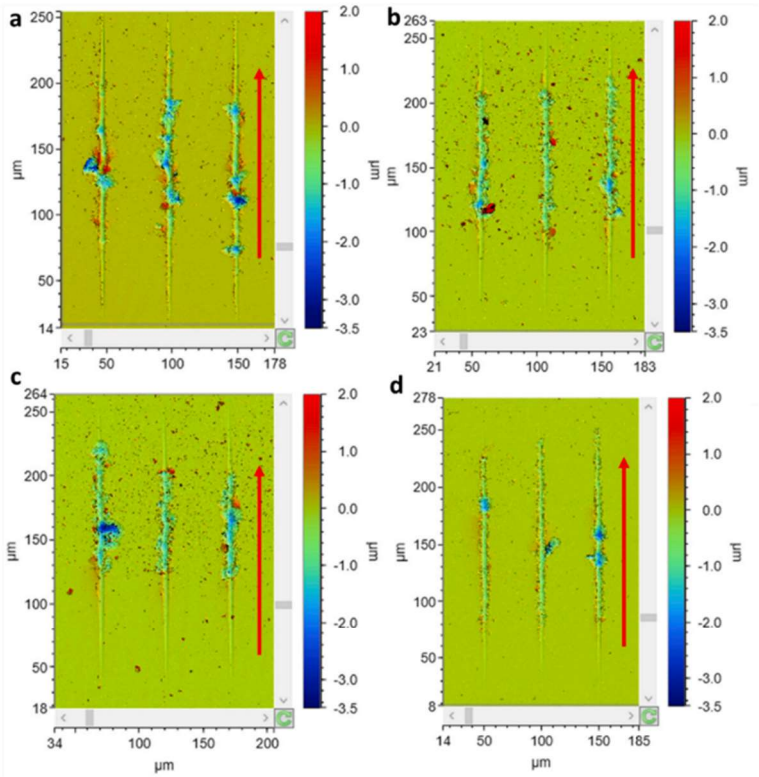


**Fig. 3.** Post mortem 3D optical profilometry scans of the ex situ 5 µm diamond scratch tests. (a) Si-reference, (b) DLC-1, (c) Si-DLC, (d) DLC-2. Red arrows represent scratch direction directions and the colour bar the relative vertical (z) height. The left-hand scratch on each coating corresponds to Fig. 2. (For interpretation of the references to colour in this figure legend, the reader is referred to the Web version of this article.)

**Table 3**
Analysis of spallation width and spallation track length for comparable 1 and 5 µm diamond scratch tests on DLC-1, DLC-2 and Si-DLC.

| Test | Average Spallation Width (µm) | Average Spallation Length (µm) |
|---|---|---|
| **DLC 1 5 µm Tip** | 10.6 ± 2.7 | 106.7 ± 3.7 |
| **Si-DLC 5 µm Tip** | 10.6 ± 4 | 88.7 ± 10.9 |
| **DLC 2 5 µm Tip** | 6.9 ± 3.7 | 159.3 ± 10.3 |
| **DLC 1 1 µm Tip** | 6.4 ± 2.1 | 52.7 ± 3.1 |
| **Si-DLC 1 µm Tip** | 7.2 ± 2 | 49.5 ± 6.4 |
| **DLC 2 1 µm Tip** | 3.2 ± 2.3 | 63.7 ± 0.6 |

Post-mortem measurement of the wear scar topography generated by the in situ DLC-1 scratch (Fig. 5), provides further insights into both the formation of pile up and the spallations that surrounded the edge of the wear scar in the later higher-load stages of the test. The depth of the wear scar seen in Fig. 5(b) is consistent with topography seen from the post-test depth scans in the ex situ tests (Fig. 2). The wear scar depth increases with applied load, with a sharp increase in depth at the onset of spallation. In regions where the DLC-1 coating has fully spallated away, plastic deformation of the Si substrate occurs down to ~1000 nm depth. The surface topography along the edge of the wear scar (Fig. 5(b), red arrow) increases in height towards the onset of spallation. This pile-up is due to the material displacement by the tip and uplift associated with cracking along the wear track. Spallation craters at the very edge of the wear scar go down to around −550nm, which is the depth of the coating in DLC-1, consistent with interfacial crack propagation. A large lateral crack at the end of the wear track (Fig. 4(h)), in effect an incomplete spallation event, generates a 1.5 µm uplift region (Fig. 5(b)). Fig. 5 (c) shows the residual surface topography across the DLC-1 wear track. Just prior to spallation, where radial cracks are propagating radially outwards from the wear track (Fig. 4(h)), pile-up forms evenly (185 nm and 189 nm) either side of the wear scar relative to scan direction (Fig. 5(a,c), orange arrow). The topography across the wear scar in the spallation zone (green arrow) demonstrates uplift at the track edges, wear down to 1 µm depth (into the Si), and a residual depth of one of the larger spallation craters of −700nm, indicating removal of the Si substrate by cracking below the DLC-1/silicon interface.

Si-DLC demonstrated very similar plastic deformation behaviour to DLC-1 during in situ SEM scratch testing. Fig. 6(a–f) shows a representative time-resolved sequence of plastic deformation occurring during a 5 µm radius diamond conical scratch test on Si-DLC. As load increased to ~190 mN during the scratch, radial cracks were initiated to the front and side of the diamond tip-DLC contact zone (Fig. 6(a and b)). Radial crack generation was associated with load fluctuations due to changes in local stress. Immediately prior to coating spallation, widening of the crack in the front of the indenter was observed (Fig. 6 (c)). This frontal crack then propagated to form a ~10 µm diameter circular subsurface lateral crack ahead of the tip (Fig. 6(d)) leading to a large spallation event. The spallation depth was down to the Si-substrate, with the lateral crack rising obliquely up through the DLC coating at its edges. The spalled coating wear fragment was ejected out of the SEM field of view.

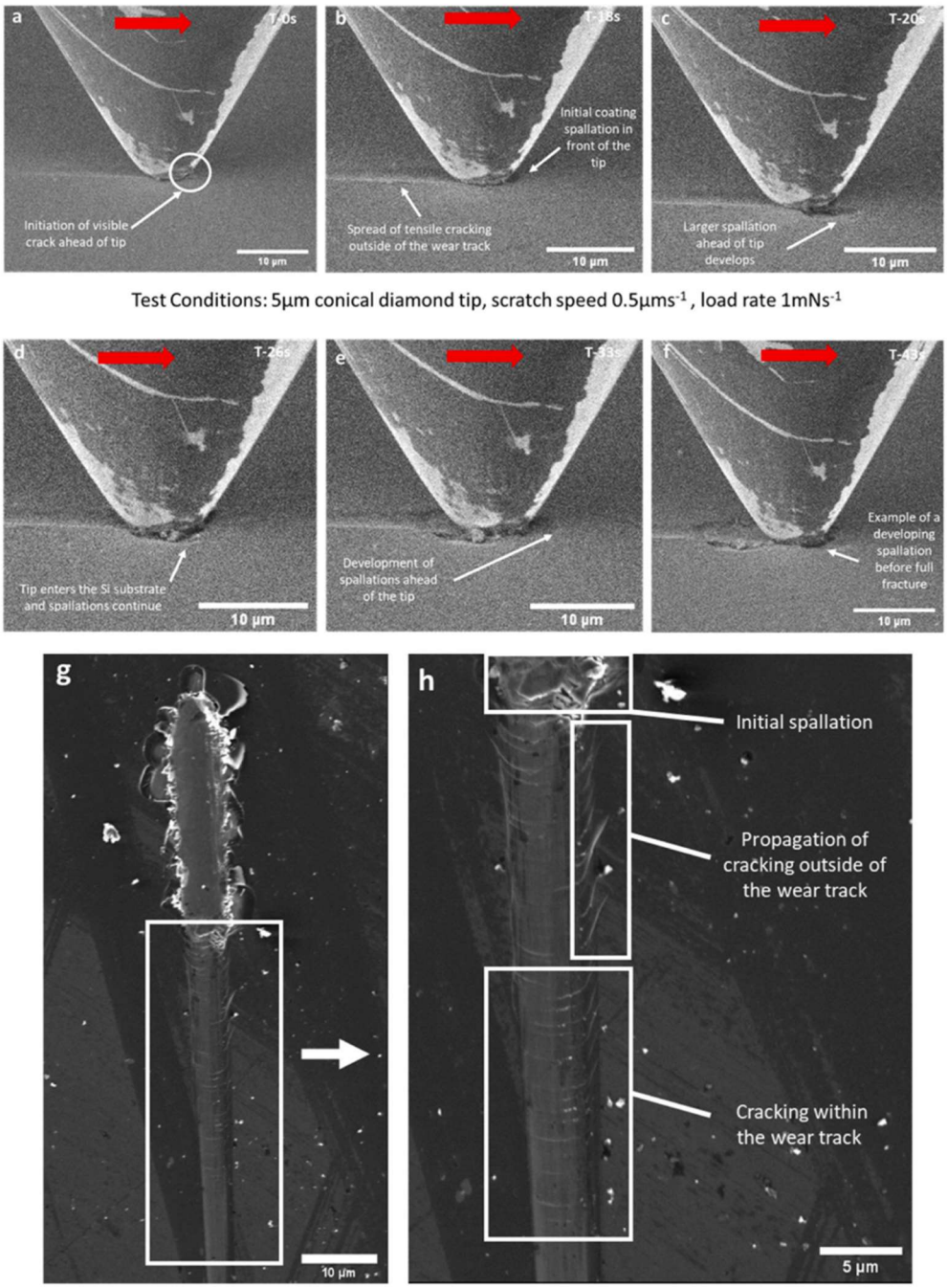


**Fig. 4.** In situ SEM 5 µm diamond tip scratch test of DLC-1. (a) Crack initiation ahead of tip (T-0s/188 mN). (b) Development of spallation ahead of the tip, and crack in (a) creating slight uplift (T-18s/206 mN). (c) Development of larger spallation ahead/to side of tip (T-20s/208 mN). (d) Tip enters the Si substrate as full coating spallation occurs (T-26s/214 mN). (e) Tip continues into substrate and further frontal spallations develop (T-33s/221 mN), (f) Continued spallation with widening of existing spallations behind the tip as it passes (T-43s/231 mN). (g,h) Annotated postmortem SEM images of the test observed in (a–f). Scratch direction given by the red arrows. Times of (a–f) are relative to (a). (For interpretation of the references to colour in this figure legend, the reader is referred to the Web version of this article.)

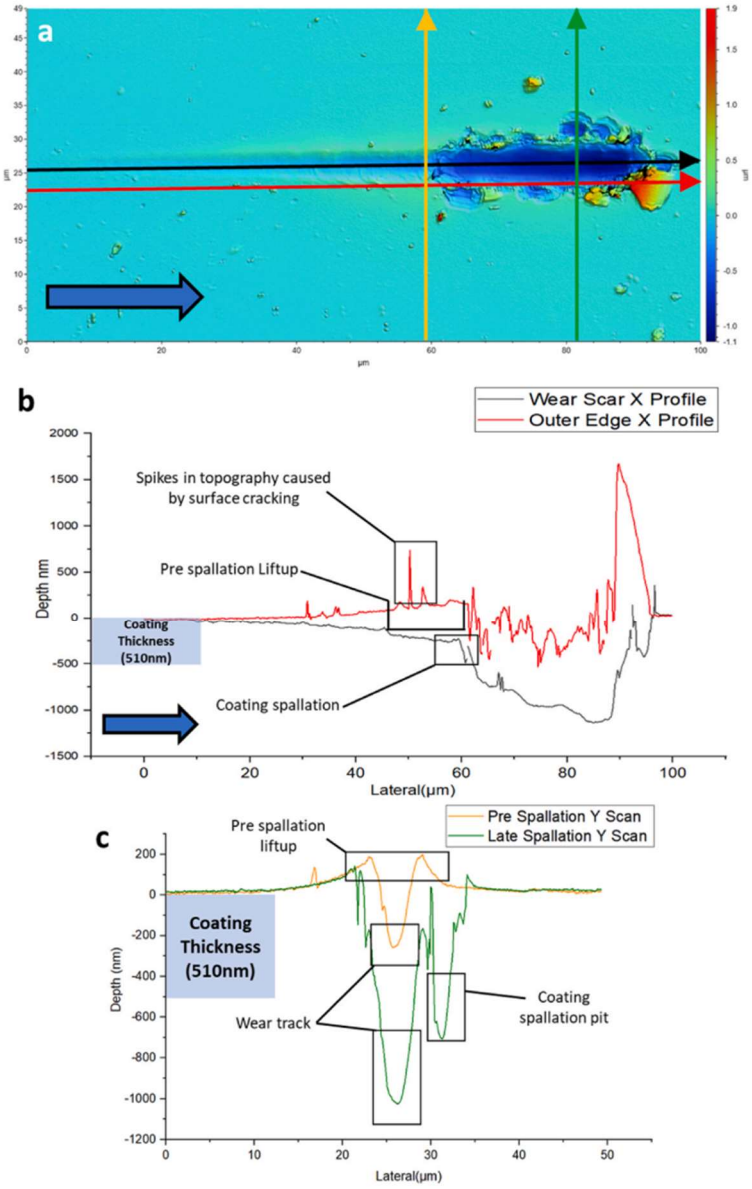


**Fig. 5.** 3D optical profiling of the DLC-1 wear track from Fig. 4. (a) Top-down view of the topographical scan with overlaid cross section lines (colour coded with arrows to indicate cross-section direction). (b) X profile scans along the length of the scratch both at the base of the wear scar (black arrow) and along the outer edge (red arrow). (c) Y profile scans, both just before spallation onset (orange arrow) and across a later stage spallation (green arrow). (For interpretation of the references to colour in this figure legend, the reader is referred to the Web version of this article.)

Without the protective Si-DLC coating the tip ploughed into the Si substrate at the site of the spallation (Fig. 6(e and f). The transition from radial cracking to spallation, and the rough surface of the spallation crater is highlighted in the post-test image of the scratch-track in Fig. 6 (g).

The behaviour of the DLC-1 and Si-DLC coatings (510 and 620 nm thickness) during scratch tests were compared to that of the thinner 260 nm DLC-2 coating. Fig. 7 shows comparative post-test SEM images taken for each of the coatings after a 5 µm radius diamond in situ scratch test. The thinner DLC-2 coating displayed some noticeable differences. The tensile cracking within the DLC-2 wear scar in the lead up to spallation onset was very limited in density, occurring predominantly in a 5 µm band just before coating spallation occurs (Fig. 7(c)). Almost no radial cracking outside the wear track was observed before spallation, and the onset of spallation of DLC-2 occurred at a lower load than for DLC-1 and Si-DLC (see Section 3.4). Additionally, for the thinner DLC-2 coating the spallation events were on average smaller in size, and with less extension outwards from the scratch track. This is consistent with the observed behaviour within the ex situ testing (Fig. 4, Table 3) where a longer, but less severe band/narrower of spallation was observed for DLC-2.

To examine the onset of spallation in more detail, focused ion beam (FIB) milling was used to cross-section a 5 µm radius diamond ex situ scratch test on DLC-1 (Fig. 8), perpendicular to the scratch direction

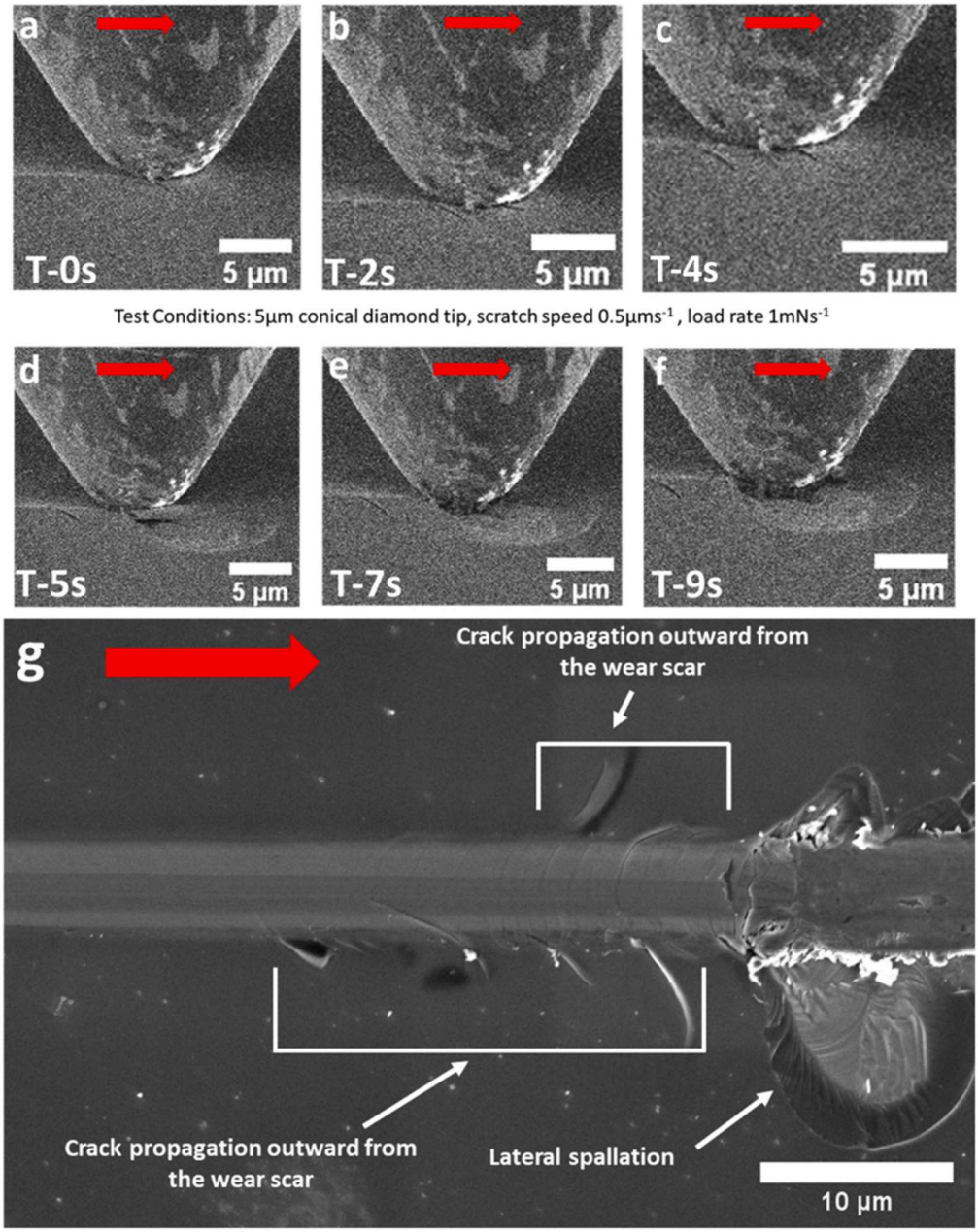


**Fig. 6.** In situ SEM 5 µm diamond tip scratch test of Si-DLC. (a) Radial crack initiation to side of tip (T-0s/190 mN). (b) Second radial crack to front-right of the contact zone (T-2s/192 mN). (c) Widening of the radial cracks propagating outwards at ~60° from scratch direction (T-4s/196 mN). (d) Propagation of a ~10 µm diameter circular subsurface lateral crack ahead of the tip from the crack seen in (c)(T-5s/197 mN). (e) Spallation of fractured coating, and the tip enters the Si substrate (T-7s/199 mN). (f) Tip begins to plough through the Si substrate (T-9s/201 mN). (g) Annotated postmortem SEM image of the test observed in (a–f). Scratch direction given by the red arrows. Times of (a–f) are relative to (a). (For interpretation of the references to colour in this figure legend, the reader is referred to the Web version of this article.)

(Fig. 8). Directly below the wear scar a microcracking zone was observed in the Si substrate at depths ~1–2 µm below the DLC coating-substrate interface (Fig. 8). Lateral cracks propagated under and beyond the scratch edges at around 0.5–1 µm depth below the DLC coating-substrate interface (Fig. 8). In the examined FIB cross-section, it can be seen that in the centre of the scratch track the DLC-1 coating has a deformed concave shape and is still conformal with the Si-substrate. However, at the edges of the scratch, transverse/radial cracks exist through the thickness of the coating, and lateral cracks have propagated both along the DLC-Si interface causing coating delamination. The

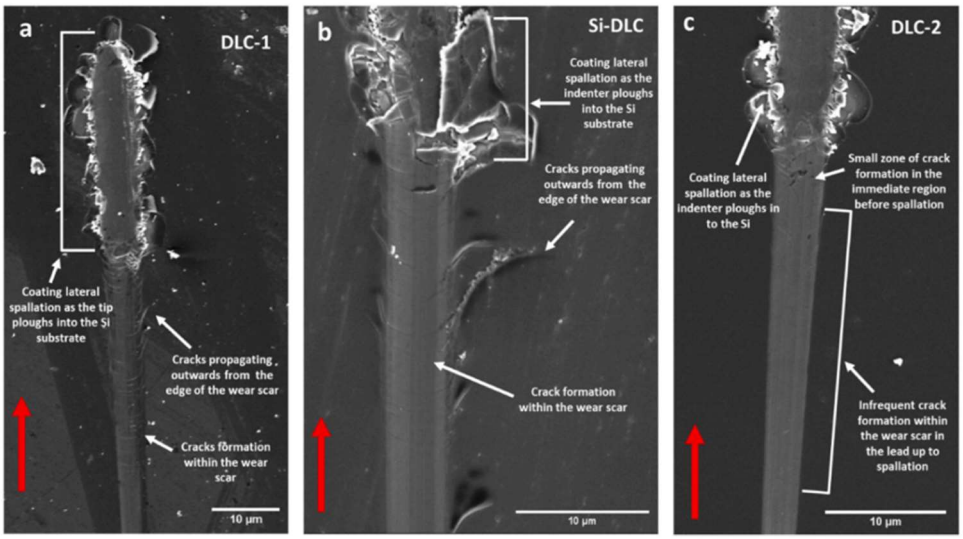


**Fig. 7.** Post-mortem SEM images of representative 5 µm diamond in situ scratch tests illustrating the onset of DLC coating spallation. (a) DLC-1, (b) Si-DLC, (c) DLC-2. Scratch directions indicated by red arrows. (For interpretation of the references to colour in this figure legend, the reader is referred to the Web version of this article.)

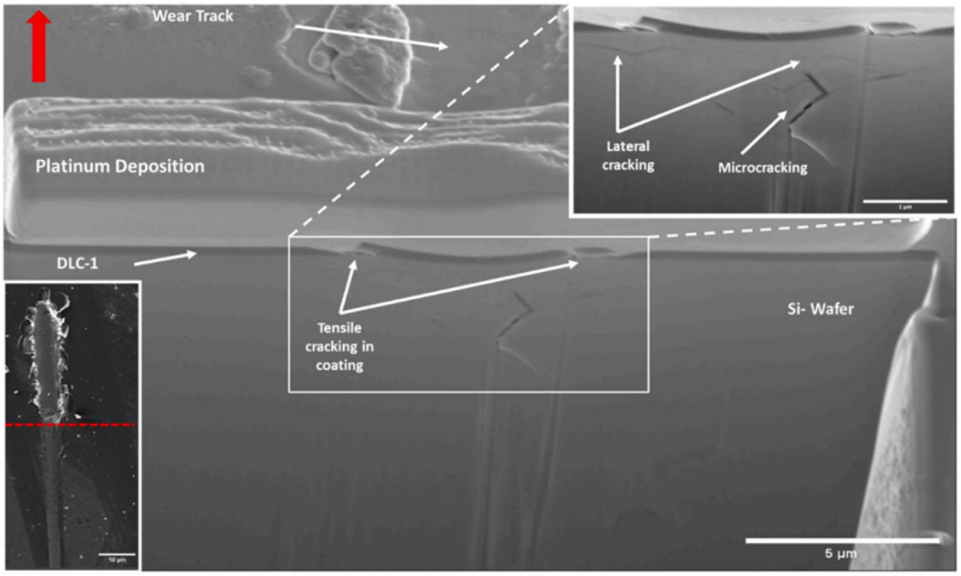


**Fig. 8.** FIB cross section of the pre spallation region of a 5 µm radius diamond ex situ scratch test of DCL-1 (position of cross section shown bottom left). An enhanced contrast image of the Si substrate cracking is displayed in the top right. The cross-section is imaged at a tilt angle of 52°. Scratch direction indicated by the red arrow. (For interpretation of the references to colour in this figure legend, the reader is referred to the Web version of this article.)

observed DLC cracking, interfacial delamination and subsurface Si cracking generate uplift in the DLC coating, consistent with the surface uplift seen via the top-down SEM images and optical profilometry (Fig. 4 (g and h), 5, 6(g) and 10).

### *3.5. In situ SEM scratch testing of DLC-1, DLC-2 and Si-DLC with 1 µm radius diamond tip*

To evaluate role of diamond asperity size on scratch deformation mechanisms, in situ SEM scratch tests were also carried out on DLC-1, DLC-2 and Si-DLC coatings using a spheroconical 1 µm radius diamond tip with a 60o cone angle. Scratch conditions for this testing were

a load rate of 1 $mNs^{-1}$, and a scratch speed of 1 $\mu ms^{-1}$.

Fig. 9(a–f) shows a representative time-resolved sequence of the plastic deformation occurring during a 1 μm radius diamond conical scratch test on DLC-1. As for the larger asperity tests, a period of plastic deformation forming a wear scar on the coating occurred prior to the onset of spallation (Fig. 9(a)). The first DLC coating spallation occurs in front of the tip (29 mN), associated with a small submicron radial crack to the side of the tip at the rear of the spallation zone (Fig. 9(b)). This small radial crack forms the edge of an uplifted section of the DLC coating that starts to form behind the tip contact zone, consistent with subsurface crack propagation also occurring to the side and rear (Fig. 9 (b)). As for the broader tip scratching, DLC spallation results in the tip ploughing into the Si substrate in the spallation crater (Fig. 9(c)).

The propagation of radial and subsurface interfacial cracks in the tensile zone behind the moving tip causes the uplifted region of DLC coating to further fracture into multiple pieces (Fig. 9(c)). One small coating fragment is pushed under a large ~3 μm 'flap' of DLC coating that is delaminated from the Si substrate but does not become full detached, with the rear edge (relative to the scratch direction) remaining attached to the rest of the coating. This incomplete spallation event results in significant ~1 μm lift up of the DLC-1 coating adjacent to the subsequent scratch track (Fig. 9(d)). Once the sharp 1 μm radius diamond tip has fully entered the Si-substrate the continued spallation mechanism is similar to that observed for the broader 5 μm radius tip scratching of DLC and Si-DLC (Figs. 4 and 6). Subsurface cracking, DLC coating spallation, and Si-substrate ploughing sequentially occur in front of the leading edge of the tip as the tip pushes itself through both the substrate and the coating (Fig. 9(d–f)). The repeated DLC-coating fracture and grooving of the Si-substrate by the sharp tip asperity generates significant third-body wear debris, which builds up around the moving tip, and is left distributed around the edge of the scratch and across the surrounding coating (from airborne brittle fracture fragments).

Post-test SEM imaging (Fig. 9(g)) highlights the residual plastic damage caused by the scratch of DLC-1, and the distribution of associated wear debris. In particular, examination of the transition zone just prior to delamination demonstrates that the onset of subsurface lateral cracking gives rise to significant residual coating lift up. For the scratch in Fig. 9, it can be seen that partial DLC coating delamination occurs on both sides of the scratch, caused by propagation of lateral cracks behind the indenter tip (Fig. 9(b–f)). Upwards protrusion of these liftup sections was quantified with topographical profilometry, with localised uplift occurring to more than 1000 nm (Fig. 10(a and b). In addition, further localised areas of uplift occur along the scratch track due to radial/lateral cracks (effectively 'incomplete' spallation) and wear debris (Fig. 10(a)).

Compared to the 5 μm tip radius scratch on DLC-1 (Fig. 5), the depth of the 1 μm scratch track reaches down further into the Si-substrate (−1400 nm, Fig. 10(b), black arrow), but the width of the deep residual groove is narrower (~2 μm) due to the sharper 1 μm radius asperity (Fig. 10(c), green arrow). The spallation craters along the very edge of the wear scar extend 2–5 μm laterally, and go down to around −500nm, which is comparable to the depth of the coating in DLC-1, again consistent with interfacial crack propagation.

Comparative post-test SEM imaging of 1 μm radius diamond in situ scratch test scratches on the three coatings, DLC-1, Si-DLC and DLC-2 (Fig. 11), highlights the modified plastic behaviour observed compared to the 5 μm radius diamond tests (Fig. 7). Both DLC-1 and Si-DLC displayed tensile cracking within the wear scar prior to spallation, but for a more limited distance. Radial cracking extending out of the scratch track was only observed directly adjacent to the onset of spallation (Fig. 11 b,d), and was associated with the significant liftup caused by subsurface lateral cracking and coating delamination in this transition zone. This indicates that once radial and lateral microcracking is initiated, the highly localised stress field associated with the sharper indenter results in rapid propagation and an abrupt transition to spallation compared to the blunter tip scratch.

The thinner DLC-2 coating once again showed very limited tensile cracking in the wear track, being limited to just before coating spallation. The onset of spallation of DLC-2 was abrupt, and also associated with residual liftup at the transition arising from partial coating delamination (Fig. 11 (f)). The average lateral extension of spallation damage of DLC-2 outwards from the 1 μm scratch track was again significantly lower than for DLC-1 and Si-DLC (Table 3), although the average length of spallation was longer. For all three DLC coatings, the spallation damage zone was much narrower for the sharp 1 μm asperity scratches than for the 5 μm radius scratching asperity (Table 3).

Post-mortem cross-sectioning of a 1 μm radius diamond in situ scratch test on DLC-1 (Fig. 12), just prior to spallation and perpendicular to the scratch direction (Fig. 12) revealed microcracking in the Si substrate. The cracking occurred ~0.5–2 μm below the DLC-1-Si coating interface (Fig. 12). Compared to the Si-substrate cracking occurring under DLC-1 scratched by a 5 μm tip (Fig. 8), the degree of observable Si microcracking was much more limited with just two cracks clearly visible. The DLC-1 was deformed in a concave manner under the scratch, and in this particular cross-section is still conformal with the Si-substrate, with no cracks along the DLC-Si interface, or through the DLC-1 coating thickness.

### 3.6. *Critical contact pressure and load at initial DLC coating spallation*

The average normal contact pressure at the point of initial DLC coating spallation was measured across all scratch tests for each sample, summarized in Fig. 13. In general, the comparable 5 μm diamond tip in situ and ex situ tests matched up well, with no significant difference found between these tests upon all samples. A higher contact pressure was required to initiate spallation in the thicker DLC-1 and Si-DLC coatings, compared to the thinner DLC-2 coating and the Si substrate. Spallation occurred at an increased contact pressure for the smaller 1 μm radius diamond asperity contact compared to the 5 μm radius diamond asperity contacts across all samples including that of the Si reference sample. For the Si reference, an observed increase from 7.6 GPa to 9.9 GPa occurred. DLC-1 increased from 11.8 GPa to 14.4 GPa, Si-DLC 10.1 GPa–15.0 GPa and DLC-2 8.4 GPa to 11.6 GPa, equivalent to increases of 30.1%, 21.7%, 48.4% and 37.6% in critical contact pressure.

The critical loads, and displacement of the diamond tip at the point of spallation, were also evaluated (Fig. 14(a and b)) to determine the influence of asperity size. All coatings showed an increase in both critical load and average tip displacement from the 1 μm–5 μm diamond tip scratch test conditions. Averaged over the scratch tests (Fig. 14), critical loads for coating spallation of DLC-1 increased from 25.8 mN to 175.8 mN, Si-DLC 34.9 mN–210.2 mN and DLC-2 23 mN–144.4 mN, with the corresponding diamond tip displacement increasing from DLC-1 517 nm–815 nm, Si-DLC 832 nm–1015 nm and DLC-2 699 nm–808 nm.

## 4. Discussion

### 4.1. *DLC coating mechanical properties*

The mechanical properties of a DLC coating are a critical factor in determining their tribological performance. For the three DLC coatings in this study, the average hardness of DLC-1 and DLC-2, 18.8 GPa and 17.5 GPa respectively (Fig. 2(c)) were in the typical range for PECVD DLC-coatings of approximately 500 nm in thickness [18]. The doped Si-DLC had a comparatively lower average hardness H = 14.2 GPa, and reduced modulus $E_r = 122 \pm 12$ GPa, in line with previous evaluations of Si doped DLCs [5,8,16]. This softening is attributed to the incorporation of the Si within the four-fold co-ordinated network, which weakens the adjacent C–C bonds, and reduces the Raman ID/IG ratio (Table 1) due to modified $sp^3/sp^2$ ratio as Si does not π bond [8,19,20]. Surface chemistry was also affected by Si doping. The Si-DLC displayed the highest surface oxygen content, 14.6 at% of XPS detected elements,

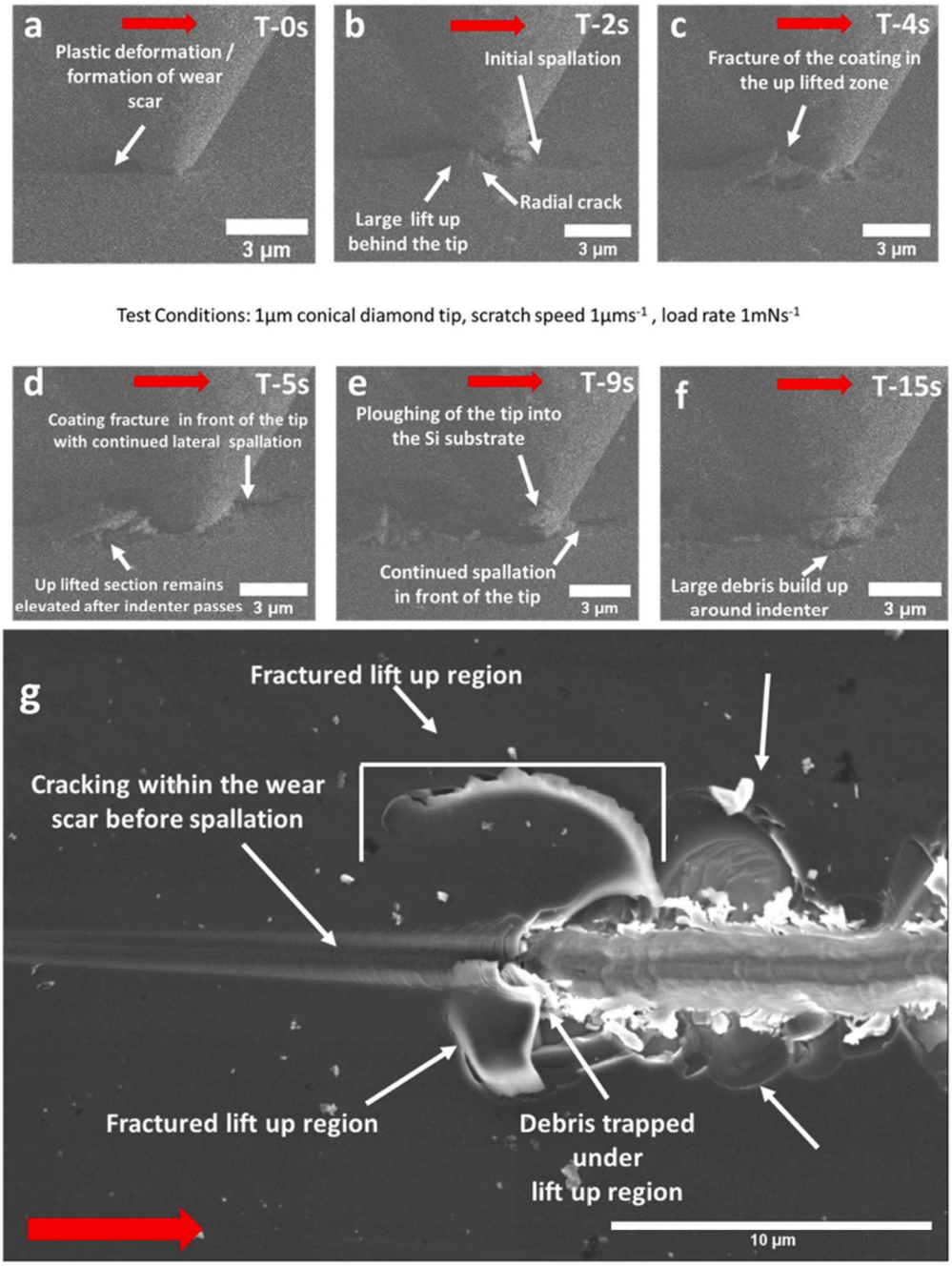


**Fig. 9.** In situ SEM 1 µm diamond scratch test of DLC-1. (a) Plastic deformation within the DLC coating forming an observable wear scar (T-0s/>29 mN. (b) Spallation ahead of the tip and subsurface fracture generates lift-up behind the tip(T-2s/29 mN). (c) The tip enters the Si substrate and fracture of the coating lift-up zone (T-4s/31 mN). (d,e) Continued DLC spallation in front of the tip (d- T-5s/32 mN)(e-T-9s/36 mN). (f) Continued spallation and Si ploughing causes buildup of DLC + Si debris around the tip (T-15s/42 mN). (g) Annotated postmortem SEM images of the test observed in (a–f). Scratch direction given by the red arrows. Times of (a–f) are relative to (a). (For interpretation of the references to colour in this figure legend, the reader is referred to the Web version of this article.)

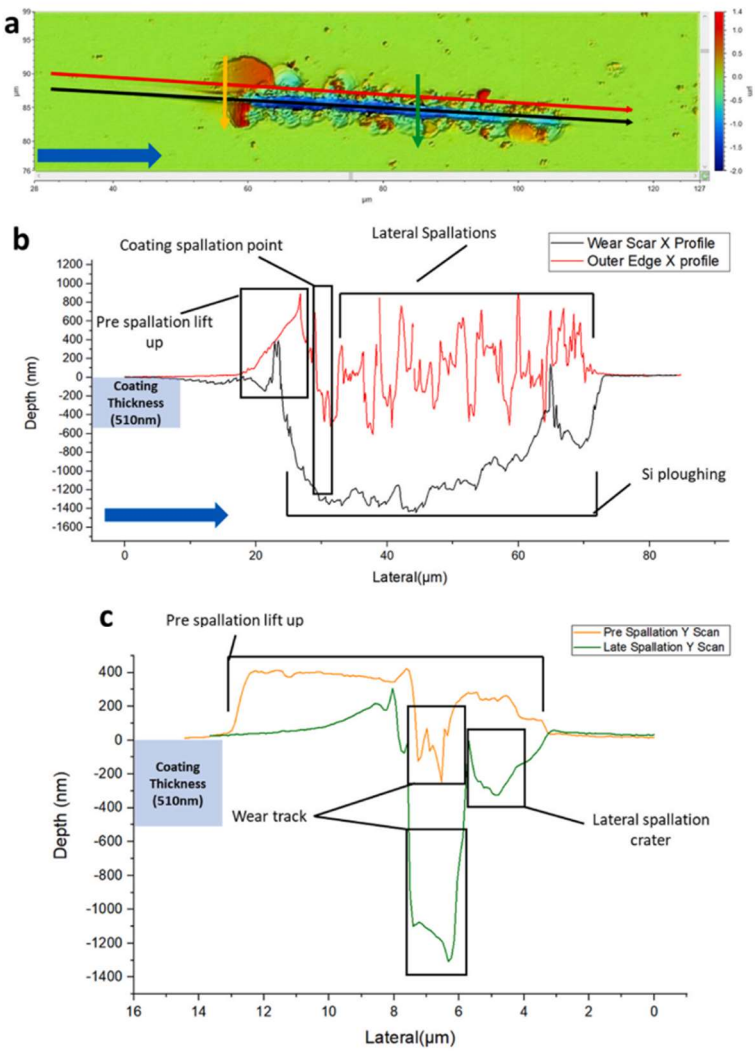


**Fig. 10.** 3D optical profiling of the DLC-1 wear track from Fig. 9. (a) Top-down view of the topographical scan with overlaid cross section lines (colour coded with arrows to indicate cross-section direction). (b) X profile scans along the length of the scratch both at the base of the wear scar (black arrow) and along the outer edge (red arrow). (c) Y profile scans, both just before spallation onset (orange arrow) and across a later stage spallation (green arrow). (For interpretation of the references to colour in this figure legend, the reader is referred to the Web version of this article.)

compared to 9.5 at% and 7.8 at% for DLC-1 and DLC-2 respectively (Table 2), due to a greater tendency to oxidise [16].

### *4.2. In situ observation of mechanisms of DLC coating deformation and fracture*

In this study DLC coatings were scratched with diamond asperities in situ in a scanning electron microscope to evaluate the dynamical mechanisms of DLC coating deformation, fracture and failure. In particular, the in situ SEM imaging of the scratches in real-time enabled for the first time high resolution analysis of crack initiation points in the vicinity of the moving contact, crack propagation under load, and spallation/ploughing dynamics to be evaluated (Figs. 4, 6 and 9).

In the early low-load stages of DLC scratches, the coating and substrate are compressed downwards leaving a visible, concave wear track behind the moving tip. As the load increases, tension in the deformed coating results in arc like (concave) cracks, with <100 nm opening, growing across the scratch track, consistent with previous studies of DLC behaviour during similar scratch tests [21–23]. With increasing normal load, post-test optical profilometry confirms increased pile-up either side of the scratch contact zone (Figs. 8 and 13). The increasing depth penetration and contact area of the tip with the deformed DLC coating, together with the onset of crack initiation, causes the dynamical coefficient of friction to increase and start to significantly fluctuate (Fig. B1).

In situ imaging identifies a key transition during the DLC scratch tests at increasing load, namely the initiation of radial cracks to the front and side of the tip-coating contact zone (Fig. 4(a, b, h), 5(b) 6(a-c, g), 7, 9(g) and 11). These cracks initially grew radially outwards and forwards from the contact zone. As the stress-field changed as the tip moved past the radial cracks, they continued to grow outwards until equilibrium was reached. Post mortem, these radials can be observed extending outwards from the wear track, particularly for the 5 μm radius diamond in situ scratch tests (Fig. 4 (g,h), 6(g) and 7).

The second key transition during the DLC scratch tests at increasing load, is the observed in situ propagation of subsurface lateral cracks from the locations of the precursor radial cracks (Fig.. 4(c), 6(d) and 9

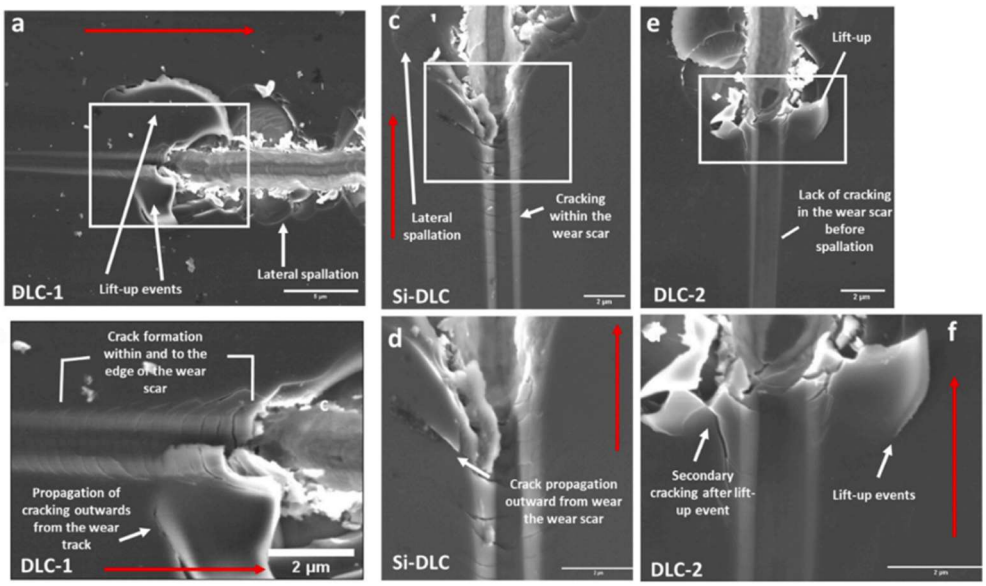


**Fig. 11.** Post-mortem SEM images of representative 1 µm diamond in situ scratch tests illustrating the onset of DLC coating spallation and coating liftup. (a,b) DLC-1, (c,d) Si-DLC, (e,f) DLC-2. Scratch directions indicated by red arrows. White boxes in (a,c,d) indicate regions enlarged in (b,d,f). (For interpretation of the references to colour in this figure legend, the reader is referred to the Web version of this article.)

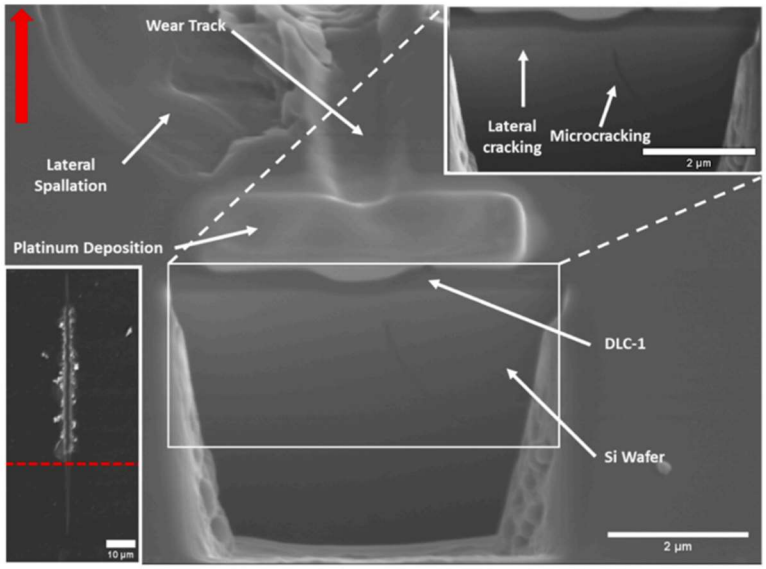


**Fig. 12.** FIB cross section of the pre spallation region of a 1 µm radius diamond in situ scratch test of DCL-1 (position of cross section shown bottom left). An enhanced contrast image of the Si substrate cracking is displayed in the top right. The cross-section is imaged at a tilt angle of 52°. Scratch direction indicated by the red arrow. (For interpretation of the references to colour in this figure legend, the reader is referred to the Web version of this article.)

(d)). This lateral cracking occurred primarily in front of, and to the side of the tip-coating contact zone. The propagation of the lateral cracks close to the DLC-coating/Si-substrate and then upwards through the coating caused the spallation of chips of coating in front of, and to the side of the tip contact zone (Fig. 4(a–f), 5, 6(d-f, g), Figs. 7 and 9(d–g), Figs.. 10 (a), Fig. 11). This directional growth behaviour gives the chip/spallation crater their distinct "tear drop" shape (Figs.. 4(g), 5(a) and 6 (g)), [24]. A-C coatings on a Si-substrate with a $H/E_r$ ratio greater than 0.09 have been observed to delaminate ahead of the contact during scratch testing [25]. In situ imaging shows that for the DLC coatings studied here the spallation is not purely a single interfacial delamination event, rather that it can be a combination of irregular radial and lateral

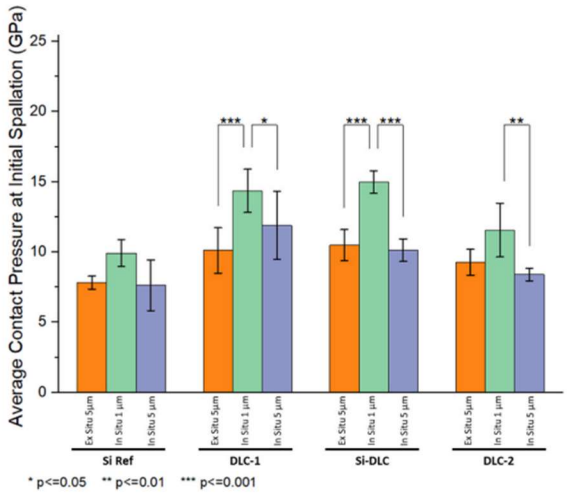


**Fig. 13.** Average normal contact pressure measured at the spallation onset of DLC-1, Si-DLC, DLC-2 coatings and Si reference sample, across all 5 µm and 1 µm diamond tip scratch tests. Asterisks indicate a statistical difference * $p < 0.05$, ** $p < 0.01$, *** $p < 0.001$, obtained using Tukey test, which computes a confidence interval for the difference between two means.

crack propagation, both through the DLC and down into the Si substrate. This results in rough spallation craters which can extend into the substrate(Figs. 5 and 10).

Importantly, for the DLC-Si-substrate systems studied here, because the spallations occurs partially ahead of the tip, as the tip moves forward, it then moves down into the softer, unprotected Si of the spallation crater and generating secondary Si cracking and ploughing. The in situ imaging confirms that the as the scratch continues, the deformation mechanism remains a multi-stage one, namely the ongoing spallation of the DLC coating ahead/to the sides of the contact zone occurs, followed by deeper Si-substrate ploughing. Further propagation of cracks behind the tip as the stresses change and then relax also occurs. This multi-stage mechanism is consistent with the post-test imaging of the residual scratch track where ploughed Si and displaced Si-debris at the edges of the wear track can be seen overlaying spallation craters (Figs. 7 and 11).

Overall, the resultant residual deformation of the DLC coatings observed post mortem after scratching exhibit many of the plastic deformation and cracking features observed in related scratch tests of thin film coatings [3,14,25–30].

For scratching with a 5 µm radius diamond tip (both in situ and ex situ), the observed plastic deformation behaviour of the DLC-1 (510 nm) and Si-DLC (620 nm) coatings was very similar. Although the Si-DLC had lower hardness (Fig. 1 (a,c)), it exhibited a slightly higher average critical load for the onset of spallation in comparison to the DLC-1 (Fig. 14(a)) resulting in a generally shorter spallation phase for the same loading regime (Figs. 2 and 3, Table 3). In comparison the thinner DLC-2 coating (260 nm) had a noticeably lower average critical load for spallation onset (Fig. 14(a)), resulting in an earlier and longer spallation phase for the same loading regime (Figs. 2 and 3, Table 3). DLC-2 had a very abrupt onset of spallation, with little to no evidence of tensile cracking in the wear scar in the lead up to spallation, and no large radial cracks which are associated with the large spallation events in DLC-1 and Si-DLC (Figs. 7 and 11). Although DLC-2 spallation onset was at a lower load (and therefore spalled for longer), the spallation events themselves were generally smaller for the thinner coating (less lateral crack propagation) creating a more localised residual wear track and smaller debris particles (Table 3). Additionally, the Si ploughing was less deep (Figs. 2 and 3), likely due to shorter spallation craters ahead of the tip and reduced frequency of deep spallation events.

### 4.3. *Influence of Si-Substrate*

In this study, the DLC coatings were deposited on Si-substrates, which is a combination relevant for microelectromechanical devices (MEMS) [28,29,31,32]. The Si is softer and less stiff compared to the DLC coatings (Fig. 1) consistent with previous studies [13], and undergoes fracture and spallation at a lower contact pressure than with a protective DLC coating (Fig. 13). In situ scratching and post-mortem observations of the substrate revealed that cracking and deformation of the Si below the coating was occurring concurrently with the surface cracking seen in the 260–620 nm thick DLC coatings (Figs. 7 and 11). FIB cross sections (Figs. 8 and 12) of DLC-1 scratch tracks illustrated that prior to spallation the silicon was susceptible to microcracking around 1 µm below the DLC coating under the compressive scratch track, and lateral cracking extending beyond the contact zone, consistent with subsurface cracking geometries observed in previous DLC and ceramic scratch evaluations [33,34]. The subsurface Si lateral cracking will contribute to the uplift observed adjacent to the scratch track prior to spallation onset (Fig. 5). Four-way scratch testing was conducted (Fig

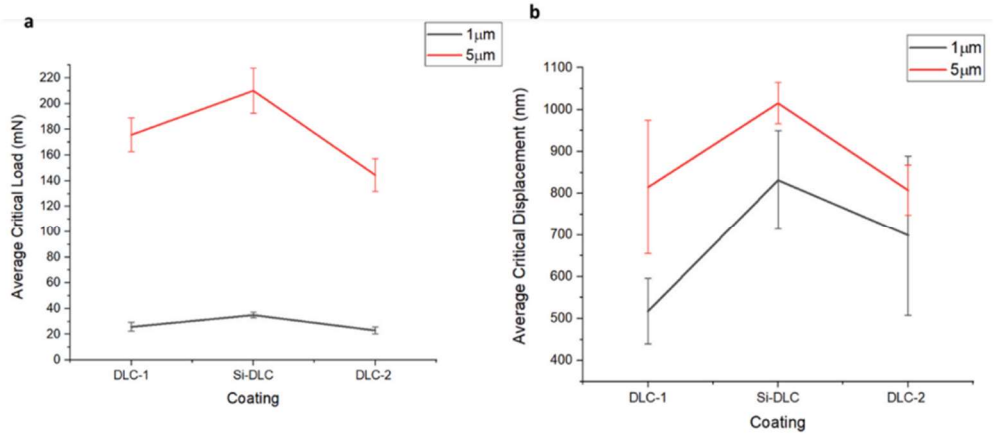


**Fig. 14.** Average critical normal loads and corresponding diamond tip displacements measured for the onset of spallation of DLC-1, Si-DLC, DLC-2 coatings, dependent on diamond tip radius (1 µm and 5 µm). (a) Average critical load of spallation. (b) Average critical tip displacement at spallation.

D1) to evaluate the influence of the orientation of the scratch direction with respect to the Silicon (001) surface, and no significant variation of critical contact pressure for spallation onset was observed. Once DLC spallation was initiated, the Si was no longer protected, and detrimental Si ploughing occurred.

### *4.4. Influence of the asperity size on contact pressure*

To evaluate role of asperity size on DLC-coating deformation mechanisms, in situ SEM scratch tests were also carried out with both 1 μm and 5 μm radius diamond tips using the same load profile. For DLC-1, Si-DLC and DLC-2 the average critical load for spallation onset with the sharp 1 μm radius asperity was significantly lower (~20%) of that required for the 5 μm radius asperity (Fig. 14(a)), and spallation occurred at a shallower tip penetration (Fig. 14(b)). Lower critical load was required due to the higher local curvature and concentration of stresses within the DLC coatings and substrate around the contact zone caused by the sharper tip. Even at significantly lower loads, the average contact pressures at the onset of spallation for the sharper 1 μm radius asperity scratch tests were measurably higher than for the broader, lower curvature 5 μm radius asperity scratch tests (Fig. 13).

For the sharper 1 μm radius asperity scratch tests, the transition of DLC-1, Si-DLC and DLC-2 from plastic deformation to cracking activation and spallation was faster, occurring at lower applied loads (Fig. 14 (a)). Furthermore, just prior to spallation of DLC-1 the underlying Si-substrate exhibited less microcracking (Figs. 8 and 12) consistent with more surface localised stresses and lower applied load. A key feature observed for the sharper asperity scratches was a lack of large radials before the onset of spallation, and a localisation of the subsequent radial/lateral cracking and associated spallations closer to the scratch track, due to the more localised stress field adjacent to the tip (Table 3). Furthermore, the transition to spallation was associated with more noticeable residual uplift of the DLC coatings (Figs. 10 and 11) compared to the broader scratches. This uplift occurs due to activation of localised radial and lateral cracking that is initially insufficient to generate a full-frontal spallation, but as the stress field changes to the side and back of the moving asperity, these cracks grow behind the tip causing a zone of DLC coating delamination, uplift, fracture, and 3rd body debris generation (Figs. 9–11).

## 5. Conclusions

The tribology of three DLC coatings, 260–620 nm thick deposited by PECVD on Si-substrates, have been evaluated in real time using in situ SEM scratch testing. The influence of DLC coating chemistry, thickness, and contact asperity size on the plastic deformation, cracking and failure mechanisms observed during scratching have been evaluated. Key conclusions are:

1. The sequence of deformation mechanisms observed in situ of DLC-coatings on Si-substrates, caused by sharp diamond asperities scratching with increasing applied load, was plastic compression, lateral uplift, concave cracking within the scratch track, radial and transverse cracking growing in front/to the side of the moving asperity, spallation, spallation crater deformation, and substrate ploughing. Further crack growth and DLC coating delamination/uplift occurred during unload behind the moving asperity.
2. The activation of radial cracks propagating in front/to the side of the tip-coating contact zone was a key transition towards DLC coating failure. Radials were associated with activation of large subsurface lateral cracks leading to spallation events.
3. Scratching by a sharper asperity (1 μm versus 5 μm radius diamond tip) activated DLC spallation at substantially lower loads/depths, with higher local pressure. The faster transition to spallation was associated with a shorter pre-spallation cracking phase, and on average spallations were smaller/localised closer to the scratch track.
4. Scratching by a sharp 1 μm radius asperity was associated with significant delamination and lift up events (up to 1 μm) of the DLC coatings just prior to spallation, arising from initiation of radial/lateral cracks ahead of the indenter, which then propagate to the rear of the moving asperity due to tensile stresses.
5. The Si-DLC exhibited a higher average critical load/tip depth required to initiate spallation compared to the undoped DLC coatings under the same scratch test conditions used. The dynamical deformation mechanisms of the DLC-1 (510 nm) and Si-DLC (620 nm) coatings were similar.

## Declaration of competing interest

The authors declare that they have no known competing financial interests or personal relationships that could have appeared to influence the work reported in this paper.

## Data availability

Data will be made available on request.


## Acknowledgements

This work was funded by a PhD Studentship (Arron Bird) from Centre for Doctoral Training in Integrated Tribology at the University of Sheffield (EP/LO1629X/1), and The Engineering and Physical Sciences Research Council (EPSRC) (Grant number EP/R001766/1) as part of the 'Friction the Tribology Enigma', a collaborative Program Grant between the Universities of Leeds and Sheffield. We wish to acknowledge the support of the Henry Royce Institute for (AB) through the Royce PhD Equipment Access Scheme enabling access to PVD coating facilities at Royce@Leeds, and access to the Micro Materials NanoTest Vantage and Bruker Contour GT at Royce@Sheffield, EPSRC Grant Number EP/R00661X/1, EP/S019367/1, EP/P02470X/1 and EP/P025285/1. Finally, we acknowledge Dr Deborah Hammond and the Sheffield Surface Analysis centre for the use of their XPS facility.

## Appendix

*A- DLC Coating Surface Roughness*

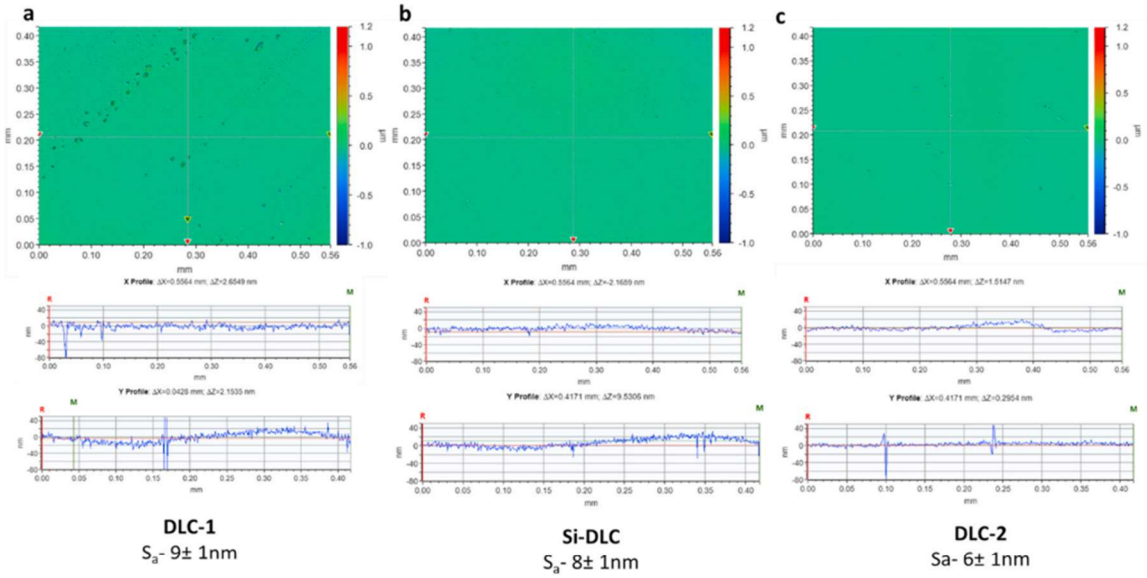


**Fig. A1.** 3D optical profilometry of the surface of each DLC coating, with representative X and Y cross sectional surface profiles and $S_a$ values given. a) DLC-1, b) Si-DLC, c) DLC-2.

*B- Ex Situ 5 μm Diamond Scratch Testing Dynamic Coefficient of Friction (CoF)*

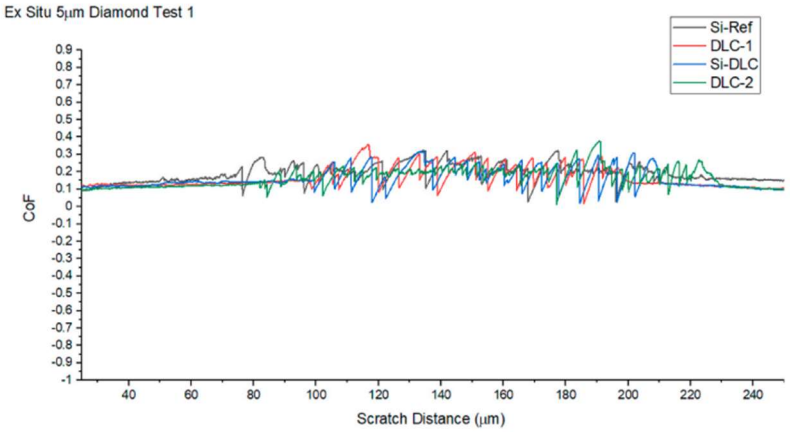


**Fig. B1.** Dynamic coefficient of friction plotted as a function of scratch distance for test 1 of the ex situ 5 μm radius diamond scratch tests on the Si-reference, DLC-1, Si-DLC, and DLC-2 coatings shown in Fig. 3.

*C- Contact Pressure at Spallation Calculation Method*

Contact pressures at the onset of DLC coating/sample spallation were calculated by the microindenter-based method proposed by Beake et al. for thin film-on-Si sliding contacts [14].

Contact depth can be given by:

$$h_p = (h_t + h_r) / 2 \quad \text{(C1)}$$

where $h_p$ is the contact depth, $h_t$ is the on-load scratch depth and $h_r$ is the residual depth from the final scan. Contact radius $a$ can then be calculated

when combined with the radius of the indenter tip ($R$).

$$a = \sqrt{2Rh_p - h_p^2} \tag{C2}$$

With contact pressure ($P_m$) then being calculated where $L$ is applied load via:

$$P_m = \frac{L}{\pi a^2} \tag{C3}$$

*D- Four-Way Directional 1 μm radius Diamond In Situ SEM Scratch Tests.* Four-way multi directional scratch testing of the DLC coatings, and Si reference, was conducted inside the SEM with a 1 μm radius diamond tip. The main aim of this was to quantify if the underlying orientation of the silicon wafer had a major impact upon the critical contact pressure at spallation. Figure D1 shows the measured critical contact pressures for three scratches in four orthogonal directions ('up', 'down', 'left', right') with respect to the underlying (001)Si wafer. Whilst some statistical fluctuations existed from test to test for spallation onset, there was no evidence of dependence of critical contact pressures on the scratch direction/silicon crystallography.

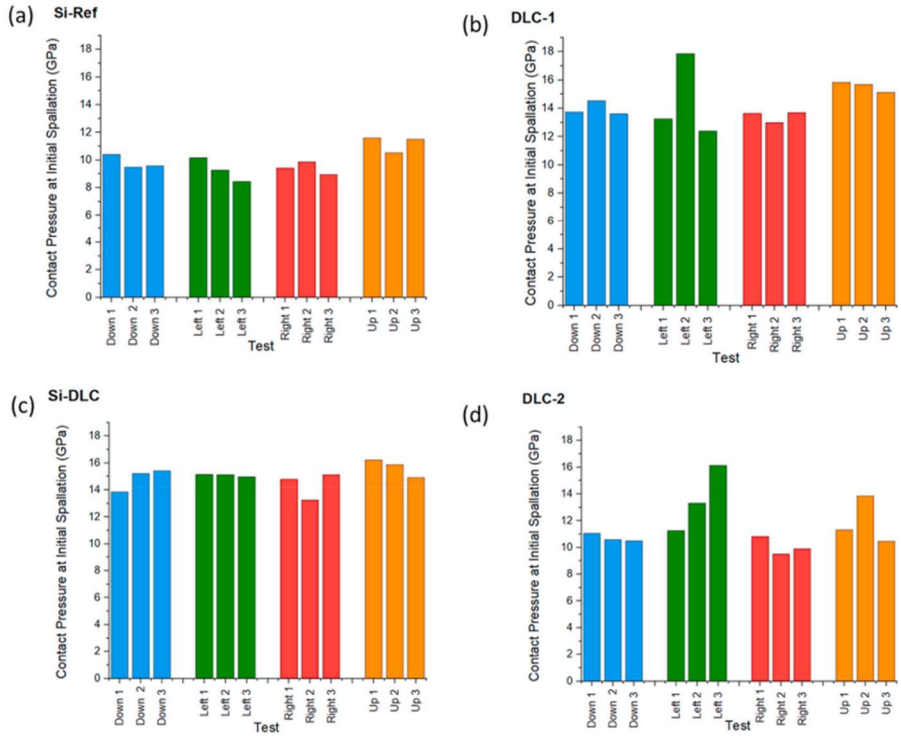


**Fig. D1.** Normal contact pressures at DLC spallation onset, measured from four-way 1 μm radius diamond tip in-situ scratch tests. (a) Si reference, (b) DLC-1, (c) Si-DLC, (d) DLC-2.

## References


[1] A. Grill, Diamond-Like Carbon: State of the Art," *Diamond and Related Materials*, 1999.

[2] S.V. Hainsworth, N.J. Uhure, Diamond like carbon coatings for tribology: production techniques, characterisation methods and applications, Int. Mater. Rev. (2007).

[3] C.A. Charitidis, Nanomechanical and nanotribological properties of carbon-based thin films: a review, Int. J. Refract. Met. Hard Mater. 28 (1) (2010) 51–70.

[4] H. Meerkamm, W. Fruth, T. Krumpiegl, C. Schaufler, Mechanical and tribological properties of PVD and PACVD wear resistant coatings, Int. J. Refract. Met. Hard Mater. (1999).

[5] J. Choi, M. Kawaguchi, T. Kato, M. Ikeyama, Deposition of Si-DLC film and its microstructural, tribological and corrosion properties, Microsyst. Technol. 13 (2007) 1353–1358.

[6] J. Wang, J. Ma, W. Huang, L. Wang, H. He, C. Liu, The Investigation of the Structures and Tribological Properties of F-DLC Coatings Deposited on Ti-6Al-4V Alloys, Surf. Coatings Technol., 2017.

[7] C. Donnet, A. Erdemir, Solid Lubricant Coatings: Recent Developments and Future Trends, Tribol. Lett., 2004.

[8] M. Bai, L. Yang, J. Li, L. Luo, S. Sun, B. Inkson, Mechanical and tribological properties of Si and W doped diamond like carbon (DLC) under dry reciprocating sliding conditions, Wear 484–485 (2021).

[9] C.B. Fischer, M. Rohrbeck, S. Wehner, M. Richter, D. Schmeißer, Interlayer formation of diamond-like carbon coatings on industrial polyethylene: thickness dependent surface characterization by SEM, AFM and NEXAFS, Appl. Surf. Sci. (2013).

[10] H. Sheng, W. Xiong, S. Zheng, C. Chen, S. He, Q. Cheng, Evaluation of the Sp3/sp2 Ratio of DLC Films by RF-PECVD and its Quantitative Relationship with Optical Band Gap, Carbon Lett., 2021.

[11] J.C. Sánchez-López, A. Fernández, Doping and alloying effects on DLC coatings, in: Tribology of Diamond-Like Carbon Films, Fundamentals and Applications, 2008, pp. 311–338.
[12] Y. Liu, A. Erdemir, E.I. Meletis, A study of the wear mechanism of diamond-like carbon films, Surf. Coating. Technol. 82 (1996) 48–56.
[13] B.D. Beake, M.I. Davies, T.W. Liskiewicz, V.M. Vishnyakov, S.R. Goodes, Nano-scratch, nanoindentation and fretting tests of 5-80nm ta-C films on Si(100), Wear 301 (1–2) (2013) 575–582.
[14] B.D. Beake, A.J. Harris, T.W. Liskiewicz, Review of recent progress in nanoscratch testing, Tribol. Mater. Surface Interfac. 7 (2) (2013) 87–96.
[15] H. Huang, H. Zhao, In situ nanoindentation and scratch testing inside scanning electron microscopes: opportunities and challenges, Sci. Adv. Mater. (2014).
[16] J.L. Lanigan, C. Wang, A. Morina, A. Neville, Repressing oxidative wear within Si doped DLCs, Tribol. Int. (2016).
[17] L. Zajíčková, V. Buršíková, V. Peřina, A. Macková, J. Janča, Correlation between SiOx content and properties of DLC:SiOx films prepared by PECVD, Surf. Coating. Technol. 174 (175) (2003) 281–285.
[18] N. Ohtake, et al., Properties and classification of diamond-like carbon films, Materials 14 (2) (2021) 315.
[19] M.H. Ahmed, J.A. Byrne, W. Ahmed, Characteristic of silicon doped diamond like carbon thin films on surface properties and human serum albumin adsorption, Diam. Relat. Mater. 55 (2015) 108–116.
[20] M. Ikeyama, S. Nakao, Y. Miyagawa, S. Miyagawa, Effects of Si content in DLC films on their friction and wear properties, Surf. Coating. Technol. 191 (1) (2005) 38–42.
[21] H. Zaidi, A. Djamai, K.J. Chin, T. Mathia, Characterisation of DLC coating adherence by scratch testing, Tribol. Int. 39 (2) (2006) 124–128.
[22] S.A. Siddiqui, G. Favaro, M. Berkes Maros, Investigation of the damage mechanism of CrN and diamond-like carbon coatings on precipitation-hardened and duplex-treated X42Cr13/W tool steel by 3D scratch testing, J. Mater. Eng. Perform. 31 (2022) 7830–7842.
[23] L. ye Huang, K. wei Xu, J. Lu, B. Guelorget, H. Chen, Nano-scratch and fretting wear study of DLC coatings for biomedical application, Diam. Relat. Mater. 10 (8) (2001) 1448–1456.
[24] X. Chen, C. Shaw, L. Gelman, K.T.V. Grattan, Advances in test and measurement of the interface adhesion and bond strengths in coating-substrate systems, emphasising blister and bulk techniques, June, Meas. J. Int. Meas. Confed. 139 (2019) 387–402.
[25] B. Shi, J.L. Sullivan, B.D. Beake, An investigation into which factors control the nanotribological behaviour of thin sputtered carbon films, J. Phys. D Appl. Phys. 41 (2008).
[26] F.O. Kolawole, A.P. Tschiptschin, S.K. Kolawole, M.A. Ramirez R, Failure of diamond-like carbon (dlc) coatings in automobile engines – a review, Proc. Eng. Sci. 1 (1) (2019) 171–180.
[27] K. Holmberg, A. Laukkanen, H. Ronkainen, K. Wallin, S. Varjus, J. Koskinen, Tribological contact analysis of a rigid ball sliding on a hard coated surface. Part I: modelling stresses and strains, Surf. Coating. Technol. 200 (12–13) (2006) 3739–3809.
[28] B.D. Beake, V.M. Vishnyakov, A.J. Harris, Nano-scratch testing of (Ti,Fe)Nx thin films on silicon, Surf. Coating. Technol. 309 (2017) 671–679.
[29] M. Larsson, M. Olsson, P. Hedenqvist, S. Hogmark, Mechanisms of coating failure as demonstrated by scratch and indentation testing of TiN coated HSS, Surf. Eng. 16 (5) (2000) 436–444.
[30] Y. Wang, X. Yu, Exploring film failure mechanism and scratch toughness characterization of diamond-like carbon film, in: Proceedings of the International Conference on Chemical, Material and Food Engineering, 2015, pp. 298–301.
[31] J.K. Luo, Y.Q. Fu, H.R. Le, J.A. Williams, S.M. Spearing, W.I. Milne, Diamond and diamond-like carbon MEMS, J. Micromech. Microeng. 17 (2007) 147–163.
[32] B.D. Beake, S.R. Goodes, B. Shi, Nanomechanical and nanotribological testing of ultra-thin carbon-based and MoST films for increased MEMS durability, J. Phys. D Appl. Phys. 42 (2009), 065301.
[33] A.J. Haq, P.R. Munroe, M. Hoffman, P.J. Martin, A. Bendavid, Deformation behaviour of DLC coatings on (111) silicon substrates, Thin Solid Films 516 (2007) 267–271.
[34] H.Z. Wu, S.G. Roberts, G. Möbus, B.J. Inkson, Subsurface damage analysis by TEM and 3D FIB crack mapping in alumina and alumina/5vol.%SiC nanocomposites, Acta Mater. 51 (1) (2003) 149–163.